INTERNATIONAL JOURNAL FOR NUMERICAL AND ANALYTICAL METHODS IN GEOMECHANICS, VOL. 20, 381–401 (1996)

FINITE ELEMENT ANALYSES OF ANISOTROPIC POROELASTICITY: A GENERALIZED MANDEL'S PROBLEM AND AN INCLINED BOREHOLE PROBLEM

L. CUI, A. H. D. CHENG AND V. N. KALIAKIN

Department of Civil Engineering, University of Delaware, Newark, Delaware 19716, U.S.A.

Y. ABOUSLEIMAN, J.-C. ROEGIERS

School of Petroleum & Geological Engineering, University of Oklahoma, Norman, Oklahoma 73019-0628, U.S.A.

SUMMARY

The finite element equations for non-linear, anisotropic poroelasticity are cast in the form of measurable engineering constants. Two problems of importance to the rock and petroleum industry are analysed by the FEM. First, the classical Mandel's problem with an extension to transversely isotropic case is investigated. Second, the problem of an inclined borehole is explored. In particular, the effect of material anisotropy on stress concentration near the wall with implication to borehole instability is examined in detail.

KEY WORDS: Poroelasticity; FEM; borehole; anisotropy; rock mechanics

INTRODUCTION

Geomaterials are often porous and saturated with fluid. Underground engineering activities such as borehole/tunnel excavation and fluid withdrawal can trigger coupled mechanical and hydraulic responses. These events are best modelled by the theory of poroelasticity. Poineered by Biot[1] in 1941, this theory has received considerable amount of attention in soil mechanics since the 1960s. In rock mechanics and petroleum engineering, the surge of interest is somewhat recent. Many important applications are now being investigated.

Using analytical tools, a number of interesting poroelastic phenomena have been revealed. Among them is the classical work of Mandel[2] and Cryer[3] which demonstrated the existence of a non-monotonic pressure response for a saturated porous specimen subject to constant external loading. Other important phenomena include the stress evolution around a borehole, with the implication to time-dependent borehole stability and *in situ* stress determination,[4–6] and the response of a fluid pressurized fracture (hydraulic fracture).[7]

Analytical solutions are generally limited to linear, isotropic problems with simple geometry. Geomaterials are often anisotropic (or transversely isotropic) with stress-sensitive material properties. A numerical tool is required for their analysis. The Finite Element Method (FEM) is well suited for this purpose.

Application of finite element to poroelasticity began in 1969 by Sandhu and Wilson[8] for the special case of incompressible fluid and solid constituents for soil mechanics applications. Since then, it has been extended to cases of compressible constituents,[9] dynamic problems,[10] non-linear and thermal-coupled problems,[11] etc. In the case of general anisotropy, the FEM presentations are often formal. It is hard to make a connection between Hooke's law coefficients and

CCC 0363-9061/96/060381-21

Received 7 September 1994
Revised 25 September 1995

measurable engineering constants. With some rare exception,[12] most formulations either do not model, or fail to recognize that the Biot's effective stress coefficient is now generalized to being a tensor, α_{ij}.

In this paper, a FEM code for coupled, anisotropic and non-linear poroelasticity is constructed. The emphasis is on anisotropy. A clear association with measurable engineering constants is established. The FEM tool is used to analyze two problems which are of critical importance to the rock and petroleum industry. First, the classical Mandel's problem, with a generalization to anisotropy (transverse isotropy), is solved. Next an inclined borehole problem is investigated, namely a borehole drilled in a direction that deviates from the principal axes of the far-field stresses. The isotropic problem is first examined and verified with an analytical solution. The effect of material anisotropy is then explored using the FEM tool. In particular, the influence of anisotropy and borehole inclination on stress concentration near the borehole is scrutinized with implication of borehole instability.

THEORY OF POROELASTICITY

The governing equations of quasi-static poroelasticity, in which the inertia effect is ignored, are presented below. The equations are cast in the incremental form such that they can be applied to incrementally non-linear materials. The equilibrium equation is expressed in terms of the rate of the total stress tensor, σ_{ij}, as

$$\dot{\sigma}_{ij,j} = 0 \tag{1}$$

where the overdot denotes the time derivative, and a comma followed by a subscript marks spatial differentiation. The elasticity sign convention, namely that positive stress denotes tension and negative compression, is used. The body force term does not appear in the above equation because a constant density is postulated. Assuming infinitesimal deformation, the strain tensor ε_{ij} is related to the displacement vector u_i as

$$\dot{\varepsilon}_{ij} = \tfrac{1}{2}(\dot{u}_{i,j} + \dot{u}_{j,i}) \tag{2}$$

The constitutive equation relates the effective stress tensor σ'_{ij} to the strain as

$$\dot{\sigma}'_{ij} = D_{ijkl}\,\dot{\varepsilon}_{kl} \tag{3}$$

where D_{ijkl} is the drained elastic modulus tensor. In the case of incrementally non-linear material, the moduli are interpreted as the tangent or the secant moduli. The condition 'drained' implies that the associated testing must be conducted under a slow loading rate such that no pore pressure buildup is observed. In the above any non-poroelastic mechanisms such as swelling, thermal or chemical effects were ignored.[11]

The effective stress law for anisotropic porous material is[13,14]

$$\dot{\sigma}_{ij} = \dot{\sigma}'_{ij} - \alpha_{ij}\dot{p} \tag{4}$$

where p is the pore pressure, and α_{ij} is the anisotropic generalized Biot's effective stress coefficient which is a second-order tensor. A constitutive equation for pore pressure is also needed, which is given by

$$\dot{p} = -M(\dot{w}_{i,i} + \alpha_{ij}\dot{\varepsilon}_{ij}) \tag{5}$$

where M is the Biot's modulus and w_i is the average displacement vector of fluid movement relative to solid skeleton. It is related to the specific flux vector q_i in groundwater flow in the form $\dot{w}_i = q_i$. It is assumed that the pore fluid flow satisfies Darcy's law:

$$\dot{w}_i = -\kappa_{ij}p_{,j} \tag{6}$$

In the above $\kappa_{ij} = k_{ij}/\mu$ is the permeability tensor, with μ denoting fluid dynamic viscosity and k_{ij} the intrinsic permeability tensor. The fluid body force term is neglected in (6); hence the pore pressure is the perturbation from the hydrostatic pressure.

The boundary conditions needed to be specified as

$$\dot{t}_i \quad \text{or} \quad \dot{u}_i \text{ given}$$

$$q \quad \text{or} \quad \dot{p} \text{ given}$$

where

$$t_i = \sigma_{ij} n_j$$

$$q = \dot{w} = \dot{w}_i n_i \tag{7}$$

are, respectively, the traction vector and the fluid flux normal to the boundary, with n_i denoting the unit outward normal vector. If the initial values of stress and pressure are not trivial, initial conditions need to be given as

$$\sigma_{ij}|_{t=0} = \sigma_{ij}^0$$

$$p|_{t=0} = p^0 \tag{8}$$

FINITE ELEMENT EQUATIONS

Following the Galerkin procedure, the weak forms of the poroelastic governing equations presented in the preceding section can be written as

$$\int_\Omega \boldsymbol{\varepsilon}^{\mathrm{T}}(\mathbf{D}\dot{\boldsymbol{\varepsilon}} - \boldsymbol{\alpha}\dot{p})\,\mathrm{d}\Omega - \int_\Gamma \mathbf{u}^{\mathrm{T}}\dot{\mathbf{t}}\,\mathrm{d}\Gamma = 0 \tag{9}$$

$$\int_\Omega \left[p\left(\boldsymbol{\alpha}^{\mathrm{T}}\dot{\boldsymbol{\varepsilon}} + \frac{\dot{p}}{M}\right) + \nabla p^{\mathrm{T}}\boldsymbol{\kappa}\nabla p \right] \mathrm{d}\Omega + \int_\Gamma p\dot{w}\,\mathrm{d}\Gamma = 0 \tag{10}$$

The following vector and matrix notations were utilized:

$$\begin{aligned}
\boldsymbol{\sigma} &= \lfloor \sigma_x \ \sigma_y \ \sigma_z \ \tau_{xy} \ \tau_{yz} \ \tau_{xz} \rfloor^{\mathrm{T}} \\
\boldsymbol{\varepsilon} &= \lfloor \varepsilon_x \ \varepsilon_y \ \varepsilon_z \ \gamma_{xy} \ \gamma_{yz} \ \gamma_{xz} \rfloor^{\mathrm{T}} \\
\mathbf{u} &= \lfloor u_x \ u_y \ u_z \rfloor^{\mathrm{T}} \\
\nabla p &= \lfloor p_{,x} \ p_{,y} \ p_{,z} \rfloor^{\mathrm{T}} \\
\mathbf{t} &= \lfloor t_x \ t_y \ t_z \rfloor^{\mathrm{T}} \\
\boldsymbol{\alpha} &= \lfloor \alpha_x \ \alpha_y \ \alpha_z \ \alpha_{xy} \ \alpha_{yz} \ \alpha_{xz} \rfloor^{\mathrm{T}} \\
\mathbf{D} &= \mathbf{D}^{\mathrm{T}} = [D_{ij}]_{6\times 6} \\
\boldsymbol{\kappa} &= \boldsymbol{\kappa}^{\mathrm{T}} = [\kappa_{ij}]_{3\times 3}
\end{aligned} \tag{11}$$

In the above we have used the engineering stress–strain notations[15] such that $\sigma_{xx} = \sigma_x$, $\sigma_{xy} = \tau_{xy}$, etc., and the superscript T denotes the operation of matrix transposition.

We approximate $\mathbf{u}$ and p by

$$\mathbf{u} = \mathbf{N}_u\{\hat{u}\}$$

$$p = \mathbf{N}_p\{\hat{p}\} \tag{12}$$

in which $\{\hat{u}\}$ and $\{\hat{p}\}$ are the column vectors of nodal values for displacement and pore pressure, respectively, and $\mathbf{N}_u$ and $\mathbf{N}_p$ are shape function matrices.[16] Thus, the finite element equation for prorelasticity is obtained as

$$\begin{bmatrix} \mathbf{K} & \mathbf{G} \\ \mathbf{G}^{\mathrm{T}} & \mathbf{L} \end{bmatrix} \begin{Bmatrix} \dot{\hat{u}} \\ \dot{\hat{p}} \end{Bmatrix} + \begin{bmatrix} \mathbf{0} & \mathbf{0} \\ \mathbf{0} & \mathbf{H} \end{bmatrix} \begin{Bmatrix} \hat{u} \\ \hat{p} \end{Bmatrix} = \begin{Bmatrix} \dot{\mathbf{F}}_1 \\ \dot{\mathbf{F}}_2 \end{Bmatrix} \tag{13}$$

where

$$\mathbf{K} = \int_\Omega \mathbf{B}_u^{\mathrm{T}} \mathbf{D} \mathbf{B}_u \, \mathrm{d}\Omega$$

$$\mathbf{G} = -\int_\Omega \mathbf{B}_u^{\mathrm{T}} \boldsymbol{\alpha} \mathbf{N}_p \, \mathrm{d}\Omega$$

$$\mathbf{L} = -\int_\Omega \frac{1}{M} \mathbf{N}_p^{\mathrm{T}} \mathbf{N}_p \, \mathrm{d}\Omega \tag{14}$$

$$\mathbf{H} = -\int_\Omega \mathbf{B}_p^{\mathrm{T}} \boldsymbol{\kappa} \mathbf{B}_p \, \mathrm{d}\Omega$$

$$\dot{\mathbf{F}}_1 = \int_\Gamma \mathbf{N}_u^{\mathrm{T}} \dot{\mathbf{t}} \, \mathrm{d}\Gamma$$

$$\dot{\mathbf{F}}_2 = \int_\Gamma \dot{w} \mathbf{N}_p^{\mathrm{T}} \, \mathrm{d}\Gamma$$

and matrices $\mathbf{B}_u$ and $\mathbf{B}_p$ are formed by differentiating $\mathbf{N}_u$ and $\mathbf{N}_p$, respectively.[16]

Because poroelasticity is a time-dependent problem, an incremental solution scheme of (13) is required. Following the standard procedure[11,17] to discretize (13) in time domain, finally, the finite element equation of anisotropic poroelasticity in incremental form is obtained as

$$\begin{bmatrix} \mathbf{K} & \mathbf{G} \\ \mathbf{G}^{\mathrm{T}} & \mathbf{L} + \Theta \Delta t \mathbf{H} \end{bmatrix} \begin{Bmatrix} \Delta \hat{u} \\ \Delta \hat{p} \end{Bmatrix} = \begin{Bmatrix} \Delta \mathbf{F}_1 \\ \Delta \mathbf{F}_2 - \Delta t \mathbf{H} \hat{p}_n \end{Bmatrix} \tag{15}$$

where Δ indicates the increment over the time interval (t^n, t^{n+1}), Θ $(0 \leqslant \Theta \leqslant 1)$ is a time-stepping weighting coefficient,[17] and

$$\Delta \mathbf{F}_1 = \int_\Gamma \mathbf{N}_u^{\mathrm{T}} \Delta \mathbf{t} \, \mathrm{d}\Gamma$$

$$\Delta \mathbf{F}_2 = \int_\Gamma \Delta w \mathbf{N}_p^{\mathrm{T}} \, \mathrm{d}\Gamma \tag{16}$$

ANISOTROPIC POROELASTIC CONSTANTS

The constitutive relations of anisotropic poroelasticity as described in (3)–(5) can be written in terms of the engineering stresses and strains, following the definitions of (11),

$$\dot{\boldsymbol{\sigma}} = \mathbf{D}\dot{\boldsymbol{\varepsilon}} - \boldsymbol{\alpha}\dot{p} \tag{17}$$

$$\dot{p} = -M(\dot{w}_{i,i} + \boldsymbol{\alpha}^{\mathrm{T}}\dot{\boldsymbol{\varepsilon}}) \tag{18}$$

Observing the symmetry in $\mathbf{D}$, there are 28 independent material coefficients for general anisotropy (21 D_{ij}, six α_{ij}, and one M).[18] However, geomaterials often exhibit certain degrees of symmetry. Two such cases, orthotropy and transverse isotropy, are examined below.

ORTHOTROPIC MATERIAL

For orthotropy, there are 13 independent material coefficients. The drained elastic modulus $\mathbf{D}$ reduces to nine coefficients:[19,20]

$$\mathbf{D} = \begin{bmatrix} D_{11} & D_{12} & D_{13} & 0 & 0 & 0 \\ D_{12} & D_{22} & D_{23} & 0 & 0 & 0 \\ D_{13} & D_{23} & D_{33} & 0 & 0 & 0 \\ 0 & 0 & 0 & G_{xy} & 0 & 0 \\ 0 & 0 & 0 & 0 & G_{yz} & 0 \\ 0 & 0 & 0 & 0 & 0 & G_{zx} \end{bmatrix} \tag{19}$$

where

$$\begin{aligned} D_{11} &= \frac{E_x E_y (E_z - E_y \nu_{zy}^2)}{A} \\ D_{22} &= \frac{E_y^2 (E_z - E_x \nu_{zx}^2)}{A} \\ D_{33} &= \frac{E_z^2 (E_y - E_x \nu_{yx}^2)}{A} \\ D_{12} &= \frac{E_x E_y (E_z \nu_{yx} + E_y \nu_{zx} \nu_{zy})}{A} \\ D_{13} &= \frac{E_x E_y E_z (\nu_{zx} + \nu_{yx} \nu_{zy})}{A} \\ D_{23} &= \frac{E_y E_z (E_x \nu_{yx} \nu_{zx} + E_y \nu_{zy})}{A} \end{aligned} \tag{20}$$

in which

$$A = E_y E_z - E_x E_z \nu_{yx}^2 - E_x E_y \nu_{zx}^2 - E_y^2 \nu_{zy}^2 - 2E_x E_y \nu_{yx} \nu_{zx} \nu_{zy} \tag{21}$$

In the above E_x, E_y and E_z are the drained Young's moduli in directions x, y and z, respectively; G_{xy}, G_{yz} and G_{zx} are shear moduli for co-ordinate planes x–y, y–z, z–x, respectively; ν_{yx}, ν_{zx} and ν_{zy} are the drained Poisson's ratios characterizing the compressive strain in the direction of the second subscript produced by a tensile stress in the direction of the first subscript (it is of interest to point out that Poisson's ratios are not symmetric, namely $\nu_{ij} \neq \nu_{ji}$). Again 9 independent material constants are counted.

The effective stress coefficients become

$$\boldsymbol{\alpha} = [\alpha_x \ \alpha_y \ \alpha_z \ 0 \ 0 \ 0]^T \tag{22}$$

It is not to our knowledge that any direct measurement of the anisotropic effective stress coefficients has been made. Hence, there may exist a gap in practical applications. However, under a special assumption of 'microisotropy', $\boldsymbol{\alpha}$ can be shown to be related to the drained elastic moduli.[14] The assumption states that the material is isotropic at the grain level such that it is characterized by two elastic coefficients, a bulk modulus K_s and a shear modulus G_s. The macroscopic anisotropy is the manifestation of the directionality of the skeleton or pore and grain structure, and not the solid constituent itself. Following the micromechanical analysis, it can be shown that $\boldsymbol{\alpha}$ is given by

$$\begin{aligned} \alpha_x &= 1 - \frac{D_{11} + D_{12} + D_{13}}{3K_s} \\ \alpha_y &= 1 - \frac{D_{12} + D_{22} + D_{23}}{3K_s} \\ \alpha_z &= 1 - \frac{D_{13} + D_{23} + D_{33}}{3K_s} \end{aligned} \tag{23}$$

The solid grain bulk modulus K_s can be measured in an unjacketed test.[21–23] One such measurement, combined with the drained elastic constants, fully defines $\boldsymbol{\alpha}$. Another useful relation is provided for the Biot's modulus M:

$$M = \frac{K_s^2}{K_s[1 + \phi(K_s/K_f - 1)] - \bar{D}/9} \tag{24}$$

where ϕ is the porosity, K_f the fluid bulk modulus and

$$\bar{D} = D_{11} + D_{22} + D_{33} + 2D_{12} + 2D_{23} + 2D_{13} \tag{25}$$

The coefficient M is hence defined with the knowledge of porosity and fluid bulk modulus.

Transversely isotropic material

In this case, there exist eight independent material constitutive constants. Five of them are the drained elastic moduli:

$$\mathbf{D} = \begin{bmatrix} D_{11} & D_{12} & D_{13} & 0 & 0 & 0 \\ D_{12} & D_{11} & D_{13} & 0 & 0 & 0 \\ D_{13} & D_{13} & D_{33} & 0 & 0 & 0 \\ 0 & 0 & 0 & G & 0 & 0 \\ 0 & 0 & 0 & 0 & G' & 0 \\ 0 & 0 & 0 & 0 & 0 & G' \end{bmatrix} \tag{26}$$

in which $G = (D_{11} - D_{12})/2$ is not independent.

By noting that $E_x = E_y = E$, $E_z = E'$, $\nu_{yx} = \nu$, $\nu_{zy} = \nu_{zx} = \nu'$, and $G_{yz} = G_{zx} = G'$, the relations with engineering constants are

$$D_{11} = \frac{E(E' - E\nu'^2)}{(1+\nu)(E' - E'\nu - 2E\nu'^2)}$$

$$D_{12} = \frac{E(E'\nu + E\nu'^2)}{(1+\nu)(E' - E'\nu - 2E\nu'^2)}$$

$$D_{13} = \frac{EE'\nu'}{E' - E'\nu - 2E\nu'^2} \tag{27}$$

$$D_{33} = \frac{E'^2(1-\nu)}{E' - E'\nu - 2E\nu'^2}$$

where E is the drained Young's modulus in the plane of isotropy (x–y plane), E' the drained Young's modulus perpendicular to that plane (z-direction), $G = E/2(1+\nu)$ the shear modulus for the plane of isotropy, G' the shear modulus normal to the plane of isotropy, ν the drained Poisson's ratio chracterizing the transverse strain reduction in the plane of isotropy due to a tensile stress in the same plane, and ν' the drained Poisson's ratio corresponding to the transverse strain reduction in the plane of isotropy due to a tensile stress normal to it.[20] Following the same microisotropy assumption, α is given by

$$\alpha_x = \alpha_y = 1 - \frac{D_{11} + D_{12} + D_{13}}{3K_s}$$

$$\alpha_z = 1 - \frac{2D_{13} + D_{33}}{3K_s} \tag{28}$$

M is defined by (24), but with $\bar{D}$ modified to

$$\bar{D} = 2D_{11} + D_{33} + 2D_{12} + 4D_{13} \tag{29}$$

EXAMPLES

Mandel's problem

The geometry of Mandel's problem is depicted in Figure 1. In this problem, an infinitely long (perpendicular to the paper) specimen with rectangular cross-section is sandwiched between two rigid, frictionless, impermeable plates, upon which a force $2F$ is applied. The side surfaces are traction free and exposed to an ambient pressure. Mandel[2] studied this problem in 1953 and demonstrated that there existed a non-monotonic pressure response. Together with the solution of Cryer,[3] which involved a three-dimensional spherical geometry, the non-monotonic pressure phenomenon was known as the Mandel–Cryer effect. Mandel's solution was restricted to the special case of incompressible solid and fluid constituents and isotropic material. The analytical solution has been extended to incorporate compressible constituents[24] and recently to transverse material isotropy.[25] To our knowledge, this latest solution[25] is the only analytical solution that involves poroelastic anisotropy. It should serve as a good benchmark for validating anisotropic poroelastic FEM codes.

Referring to Figure 1, the axis of material rotational symmetry is the z-axis. Plane strain conditions are assumed in the y-direction (perpendicular to the paper). The following set of poroelastic properties are chosen: $E_x = E_y = E = 5{\cdot}5 \times 10^3$ MPa, $E_z = E' = 3{\cdot}0 \times 10^3$ MPa, $G_{zx} = G_{yz} = G' = 1{\cdot}5 \times 10^3$ MPa, $\nu_{yx} = \nu = 0{\cdot}18$, $\nu_{zx} = \nu_{zy} = \nu' = 0{\cdot}3$, $K_s = 9{\cdot}0 \times 10^3$ MPa, $K_f = 3{\cdot}0 \times 10^3$ MPa, $\phi = 0{\cdot}2$, $\kappa_x = \kappa_y = 0{\cdot}2 \times 10^{-3}$ m^2/MPa day, $\kappa_z = 0{\cdot}4 \times 10^{-3}$ m^2/MPa day.

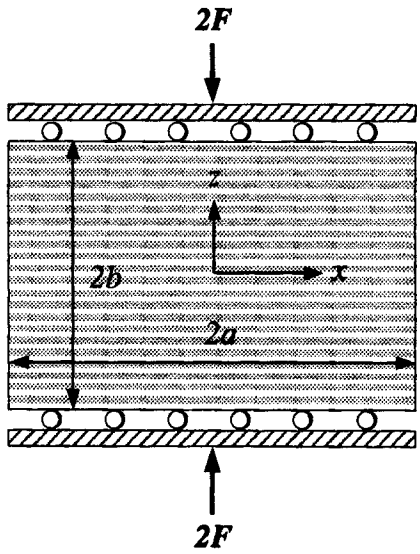

Figure 1. Mandel's problem

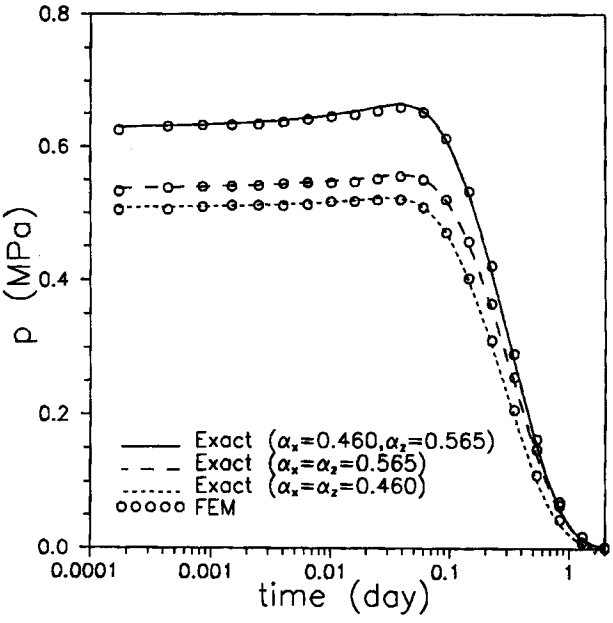

Figure 2. Mandel's problem: pore pressure history at the specimen centre $(x, y, z) = (0, 0, 0)$

Based on (24), (28) and (29), other poroelastic constants are evaluated as $M = 10{\cdot}1 \times 10^3$ MPa, $\alpha_x = \alpha_y = 0{\cdot}460$, $\alpha_z = 0{\cdot}565$.

We arbitrarily specify that the specimen dimension as $a = 1$ m and $b = 1$ m. For the finite element solution, the two-dimensional problem is solved as a three-dimensional one. We take the advantage of quarter symmetry about the x and z axes. A cube of 1 m × 1 m × 1 m is used with proper boundary conditions to ensure the plane strain condition in the y-direction. The problem domain is discretized using $10 \times 2 \times 5$ (in the x, y and z directions) 8-node isoparametric brick elements. The force is given as $F = 1$ MPa m. The pore pressure history at the center of the specimen is shown in Figure 2. The exact solution, whose expressions are presented in Reference 25, is displayed by a solid line. The FEM solution is plotted in circular symbols. Excellent agreement is observed. Notice that the pore pressure instantly raises up to a value that is characterized by the Skempton's effect. It then continues to increase for a short time before declining. This type of non-monotonic pressure response is a special feature of poroelasticity.

To demonstrate the importance of correctly modelling the anisotropic effective stress coefficient, two additional cases are solved in which, α only is considered isotropic. In the first case, the lower of the two anisotropic values is used such that $\alpha_x = \alpha_y = \alpha_z = 0{\cdot}460$, and in the second case, the higher value is adopted, $\alpha_x = \alpha_y = \alpha_z = 0{\cdot}565$. The results are also presented in Figure 2. The exact solutions (in short and long dashes) and the FEM solutions (in symbols) are again in excellent agreement. We observe that the trend of pore pressure response is somewhat unexpected. Following engineering intuition, one would expect that the anisotropic case to be bounded by the two isotropic cases, respectively, using the upper and lower bound values. Figure 2 shows that this is not the case. The pore pressure predicted by the anisotropic case is significantly higher than either of the isotropic solutions.

The evolution of vertical displacement, u_z at the centre of the rigid of plate is presented in Figure 3. The well-known consolidation behaviour manifests itself. Again, the three cases of using

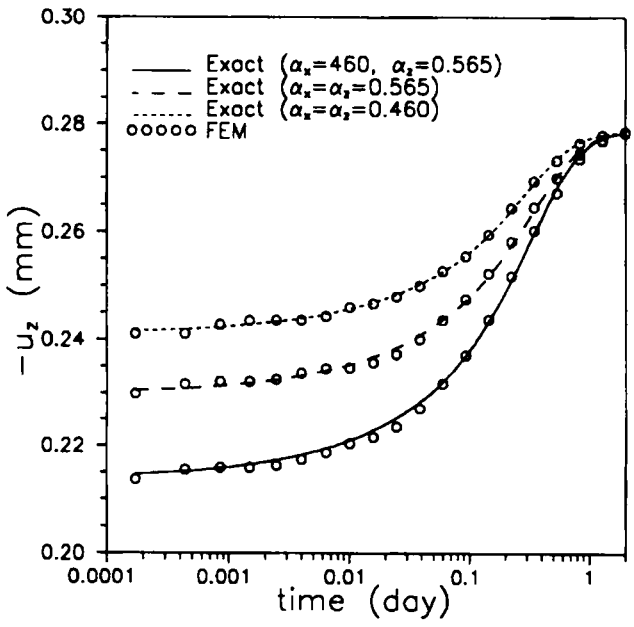

Figure 3. Mandel's problem: Evolution of vertical displacement at the centre of top plate $(x, y, z) = (0, 0, b)$

different α values are shown. At small times, the differences in settlement among the three cases are more pronounced. Again it can be observed that the isotropic cases using the upper and lower α values do not form the upper and lower bounds for the anisotropic case. As time gets large the excess pore pressure vanishes. The values of α becomes inconsequential in the evaluation of effective stress. The final settlement hence converges to the same value.

Inclined borehole problem

The inclined borehole problem is referred to a borehole drilled with its axis inclined to the principal axes of the far-field uniform stresses (Figure 4). The formation extent and the borehole length are both considered infinite. Borehole inclination is either a result of unintentional deviation, or a controlled practice that eventually leads to a horizontal well. Inclined and

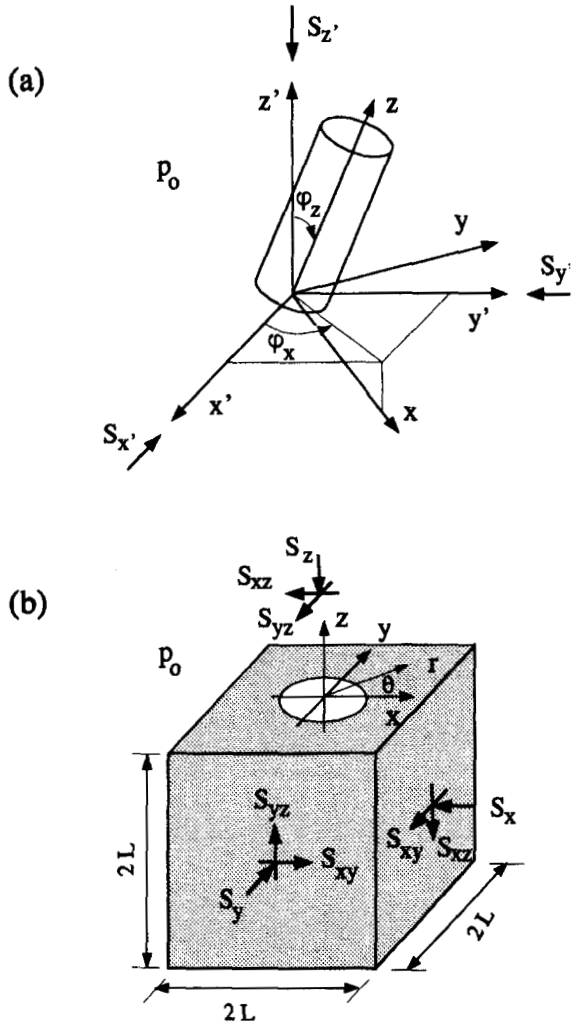

Figure 4. Inclined borehole problem

horizontal drilling is an emerging technology in the petroleum industry. Its analysis has attracted a considerable amount of attention.[26,27]

In a formation of infinite extent the Cartesian co-ordinate system $x'y'z'$ is chosen to coincide with the principal axes of the *in situ* compressive stresses, respectively, designated as $S_{x'}$, $S_{y'}$ and

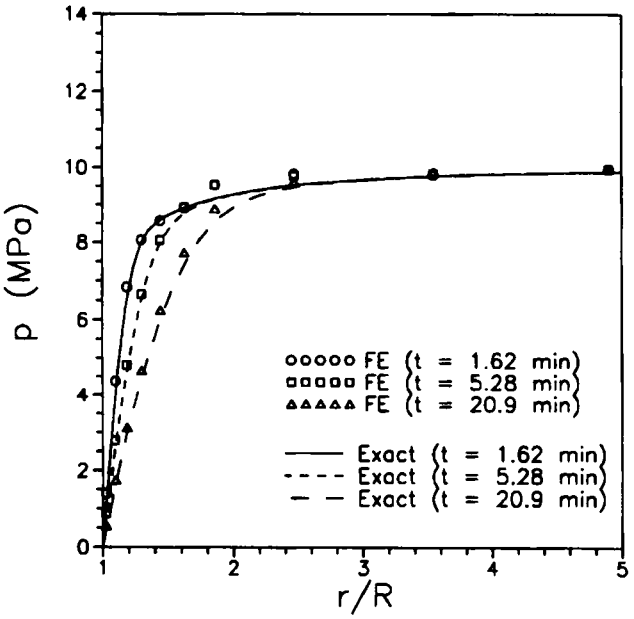

Figure 5. Pore pressure distribution along $\theta = 6.2°$, for $\varphi_z = 70°$, isotropic case

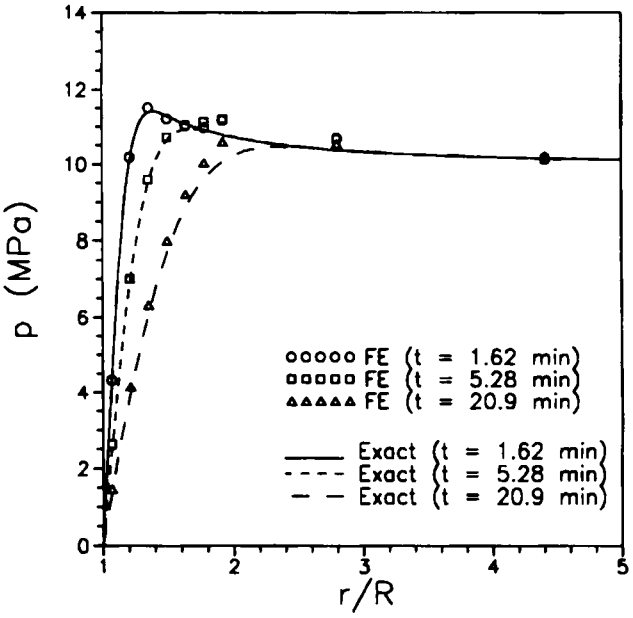

Figure 6. Pore pressure distribution along $\theta = 84.7°$, for $\varphi_z = 70°$, isotropic case

$S_{z'}$ in Figure 4(a). The virgin pore pressure is p_0. The borehole is defined by a local co-ordinate system xyz with the borehole axis coinciding with the z-axis. The local system is formed by a rotation of an azimuth angle φ_x about the z'-axis, and then by an inclination of a zenith angle φ_z toward the x-axis. See Figure 4(a) for the illustration.

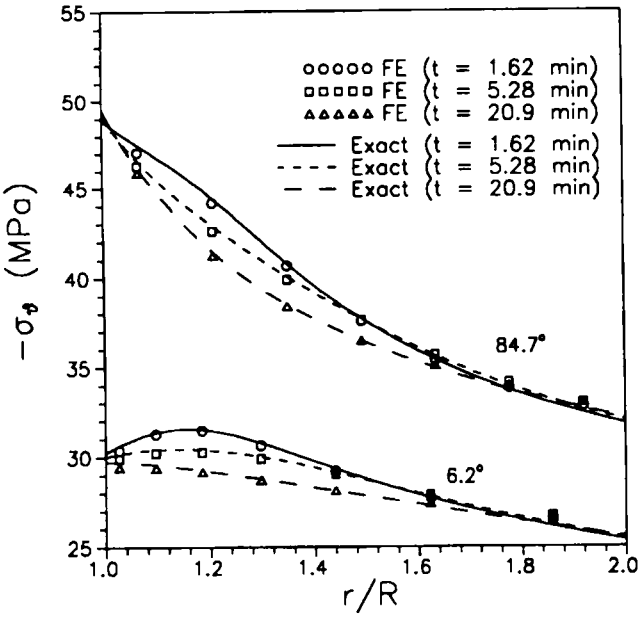

Figure 7. Tangential stress distribution around the borehole, for $\varphi_z = 70°$, isotropic case

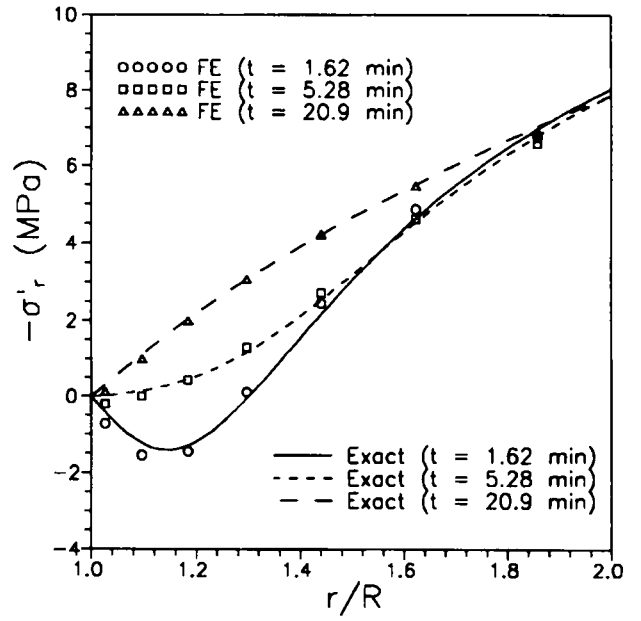

Figure 8. Effective radial stress distribution, along $\theta = 6.2°$, for $\varphi_z = 70°$, isotropic case

For the convenience of visualization and finite element meshing, the local co-ordinate system is chosen to portray the solution domain, see Figure 4(b). The *in situ* stresses are converted to the local co-ordinate system via the transformation[28]

$$\begin{Bmatrix} S_x \\ S_y \\ S_z \\ S_{xy} \\ S_{yz} \\ S_{xz} \end{Bmatrix} = \begin{bmatrix} l_{xx'}^2 & l_{xy'}^2 & l_{xz'}^2 \\ l_{yx'}^2 & l_{yy'}^2 & l_{yz'}^2 \\ l_{zx'}^2 & l_{zy'}^2 & l_{zz'}^2 \\ l_{xx'}l_{yx'} & l_{xy'}l_{yy'} & l_{xz'}l_{yz'} \\ l_{yx'}l_{zx'} & l_{yy'}l_{zy'} & l_{yz'}l_{zz'} \\ l_{zx'}l_{xx'} & l_{zy'}l_{xy'} & l_{zz'}l_{xz'} \end{bmatrix} \begin{Bmatrix} S_{x'} \\ S_{y'} \\ S_{z'} \end{Bmatrix} \tag{30}$$

where

$$\begin{bmatrix} l_{xx'} & l_{xy'} & l_{xz'} \\ l_{yx'} & l_{yy'} & l_{yz'} \\ l_{zx'} & l_{zy'} & l_{zz'} \end{bmatrix} = \begin{bmatrix} \cos\varphi_x \cos\varphi_z & \sin\varphi_x \cos\varphi_z & -\sin\varphi_z \\ -\sin\varphi_x & \cos\varphi_x & 0 \\ \cos\varphi_x \sin\varphi_z & \sin\varphi_x \sin\varphi_z & \cos\varphi_z \end{bmatrix} \tag{31}$$

These stresses and the pore pressure p_0 are prescribed at $r \to \infty$, where r is the radial distance from the borehole axis. At the borehole wall, the surface tractions and pore pressure are assumed to vanish at the instant of excavation

$$\sigma_r = \tau_{r\theta} = \tau_{rz} = p = 0; \quad \text{at } r = R \tag{32}$$

where R is the borehole radius.

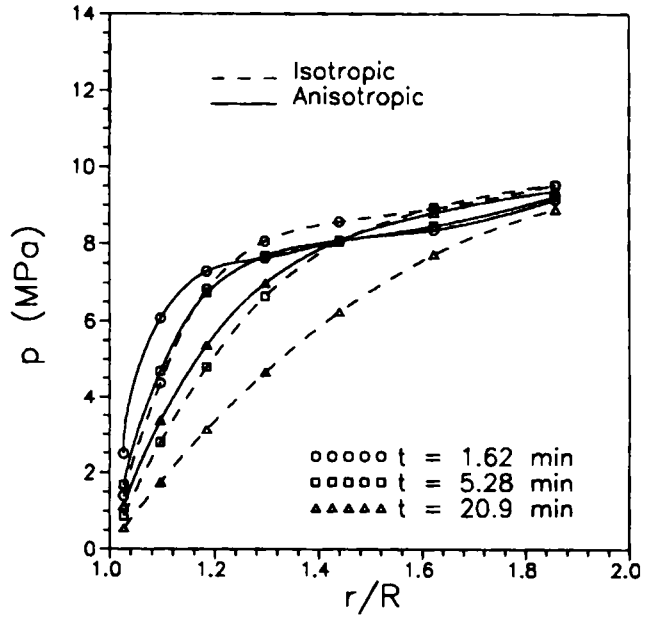

Figure 9. Comparison of pore pressure at $\theta = 6.2°$ for isotropic and anisotropic cases, $\varphi_z = 70°$

In the finite element solution the common approach of subtracting the constant far-field stresses and pore pressure from the field quantities is taken. The boundary conditions are thus modified. On all the outer surfaces of the finite domain, shown in Figure 4(b), all tractions vanish. For the fluid conditions, zero pore pressure is prescribed at the side surfaces. At the top and

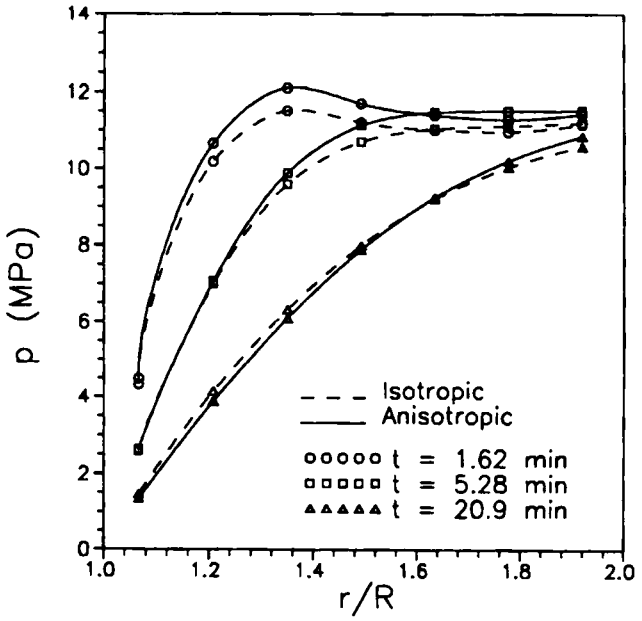

Figure 10. Comparison of pore pressure at $\theta = 84.7°$ for isotropic and anisotropic cases, $\varphi_s = 70°$

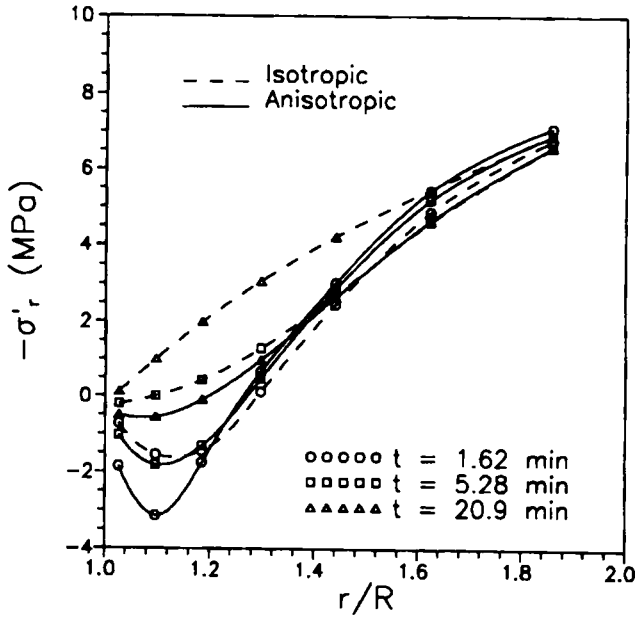

Figure 11. Comparison of effective radial stress at $\theta = 6.2°$ for isotropic and anisotropic cases, $\varphi_s = 70°$

bottom surfaces, the no flux condition, $q = 0$, is imposed. At the borehole wall, the following conditions are given:

$$\sigma_r = \frac{S_x + S_y}{2} + \frac{S_x - S_y}{2}\cos 2\theta + S_{xy}\sin 2\theta$$

$$\tau_{r\theta} = S_{xy}\cos 2\theta - \frac{S_x - S_y}{2}\sin 2\theta$$

$$\tau_{rz} = S_{xz}\cos\theta + S_{yz}\sin\theta \tag{33}$$

$$p = -p_0$$

After solving this problem, the final solution is obtained by adding back the constant background stresses and pressure.

In this example, the following conditions are used. The borehole is assumed to be drilled in the x'–z' plane ($\varphi_x = 0$) with an inclination angle $\varphi_x = 70°$. This orientation introduced symmetry about the x'–z' plane, hence only half of the domain is analyzed by the FEM. Referring to Figure 4(b), the size of the domain is given by $L = 100$ cm. The radius of the borehole is assumed to be $R = 10$ cm. Along the z-direction, the domain is divided into 7 layers. The mesh is graduated in the radial direction. A total of 1344 8-node isoparametric brick elements are used.

The *in situ* stresses and pore pressure are $S_{x'} = 29$ MPa, $S_{y'} = 20$ MPa, $S_{z'} = 25$ MPa, and $p_0 = 10$ MPa. A set of material properties reported by Aoki *et al.*[29] for a transversely isotropic Trafalgar Shale is adopted here: $E_u = 22{\cdot}0$ GPa, $E'_u = 18{\cdot}8$ GPa, $G' = 7{\cdot}23$ GPa, $\nu_u = 0{\cdot}27$, $\nu'_u = 0{\cdot}34$, $B_{x'} = 0{\cdot}51$, and $B_{z'} = 0{\cdot}63$. These measurements represent the only set of anisotropic poroelastic data that we are aware of. In the above, the subscripts u denote the undrained properties, and $B_{x'}$ and $B_{z'}$ are the anisotropic components of the Skempton's pore pressure coefficient, B. For convenience, the plane of material rotational symmetry x'–y' is chosen to coincide with the principal stress axes.

As indicated earlier, eight independent coefficients are needed to characterize transverse isotropy, yet only seven measurements were reported above. By adopting the microisotropy assumption given by (28), the seven coefficients become sufficient to define the material fully. All other coefficients are not independent. They can be evaluated from the micromechanical relations and some of them are listed below: $E = 20{\cdot}6$ GPa, $E' = 17{\cdot}3$ GPa, $\nu = 0{\cdot}189$, $\nu' = 0{\cdot}246$, $G = 8{\cdot}66$ GPa, $M = 15{\cdot}8$ GPa, $\alpha_x = 0{\cdot}733$, $\alpha_z = 0{\cdot}749$, $K_s = 48{\cdot}2$ GPa, $D_{11} = 24{\cdot}1$ GPa, $D_{12} = 6{\cdot}8$ GPa, $D_{13} = 7{\cdot}62$ GPa, $D_{33} = 21{\cdot}0$ GPa, and $D_{55} = 7{\cdot}23$ GPa.

The intrinsic permeability was not measured in Aoki *et al.*[29] The following estimates: $k_{x'} = 1 \times 10^{-7}$ darcy and $k_{z'} = 1 \times 10^{-8}$ darcy were provided, with the viscosity for water given as $\mu = 0{\cdot}001$ Pa.s. The permeability anisotropy ratio 1 : 10 used here is somewhat conservative as compared to those reported in the literature, e.g., 1 : 47 in Shah *et al.*[30] and 1 : 14 in Zuber *et al.*[31]

Although an anisotropic data set was introduced in the above, for verification purposes, and also a basis for comparison of the anisotropic effects was built. The first problem solved assumes isotropy. For the isotropy case, a subset of the above is used: $E = 20{\cdot}6$ GPa, $\nu = 0{\cdot}189$, $M = 15{\cdot}8$ GPa, $K_s = 48{\cdot}2$ GPa, $k = 1 \times 10^{-7}$ darcy, which leads to $\alpha = 0{\cdot}771$ and $B = 0{\cdot}596$.

In Figure 5 the pressure distribution in the radial direction at the angle $\theta = 6.2°$ is presented at three different times. (See Figure 4 for the illustration of θ.) In Figure 6 the same quantity is shown at the angle $\theta = 84{\cdot}7°$. Note that $\theta = 0°$ is located on the plane of inclination, i.e. the x–z plane. Since $\varphi_x = 0°$ in the current case, it coincides with the x'–z' plane. $\theta = 90°$ is in the direction of y, and also y'axis. The selection of the two angles 6.2 and 84.7°, rather than 0 and 90° is dictated by the nodal location of the FEM mesh. Observe that the pore pressure response in the near field is larger at 84·7° than at 6·2°, because there exists a larger far-field compressive stress normal to the

90° direction, than at 0°. We also note that at 84·7° a pressure peak is found at a small distance inside the wall at small times. At large distance, the pore pressure approaches asymptotically to the far-field value of 10 MPa. As a verification of the solution, the FEM result is displayed together with a recently obtained analytical solution.[32] We observe that despite the sharp changes of pressure near the wellbore, the performance of the FEM solution is quite satisfactory.

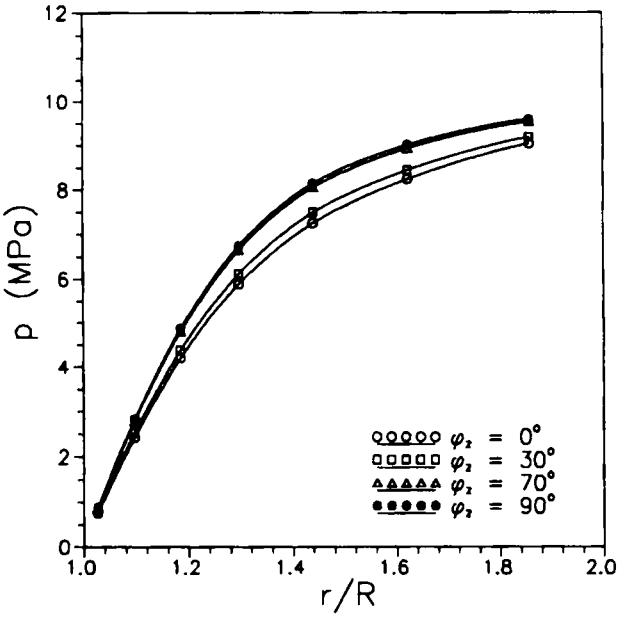

Figure 12. Effect of borehole inclination on pressure response, at $t = 5.28$ min, $\theta = 6.2°$, for isotropic case

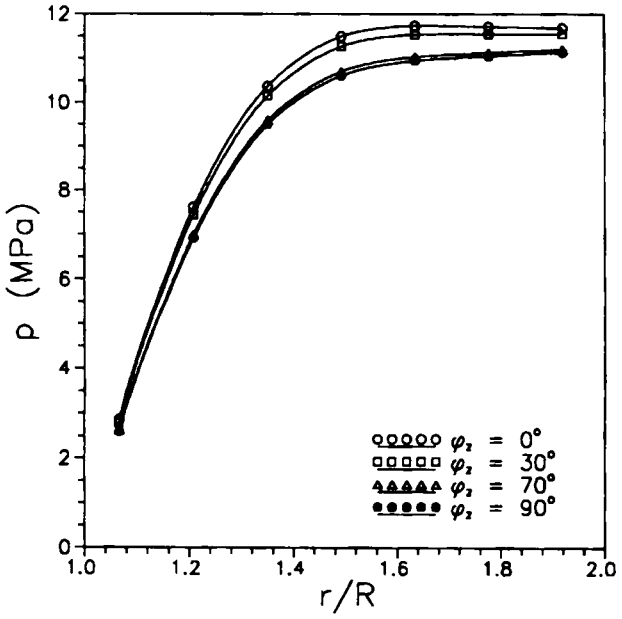

Figure 13. Effect of borehole inclination on pressure response, at $t = 5.28$ min, $\theta = 84.7°$, for isotropic case

Figure 7 shows the compressive tangential stress $-\sigma_\theta$ as a function of the radial distance and time for the two angles, $\theta = 6{\cdot}2$ and $84{\cdot}7°$. At $84{\cdot}7°$ we observe a significant increase in stress level from the far-field value approaching the borehole. The stress concentration is less pronounced at $6{\cdot}2°$. We again note the good comparison between the FEM and the exact solution.

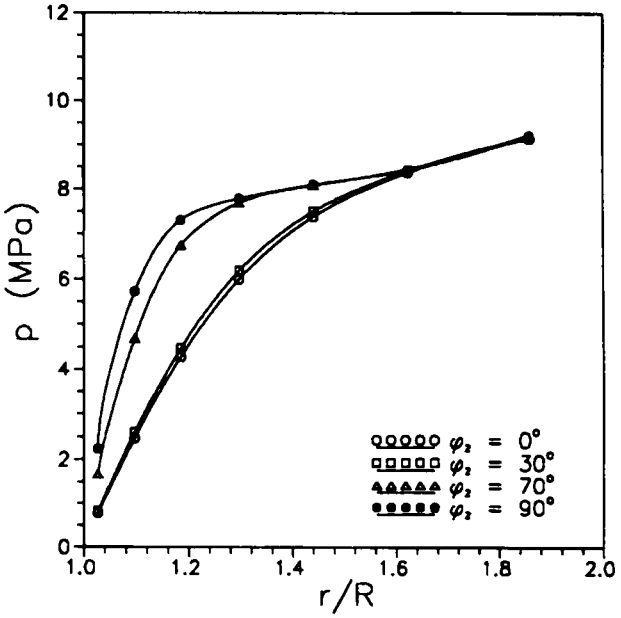

Figure 14. Effect of borehole inclination on pressure response, at $t = 5.28$ min, $\theta = 6.2°$, for anisotropic case

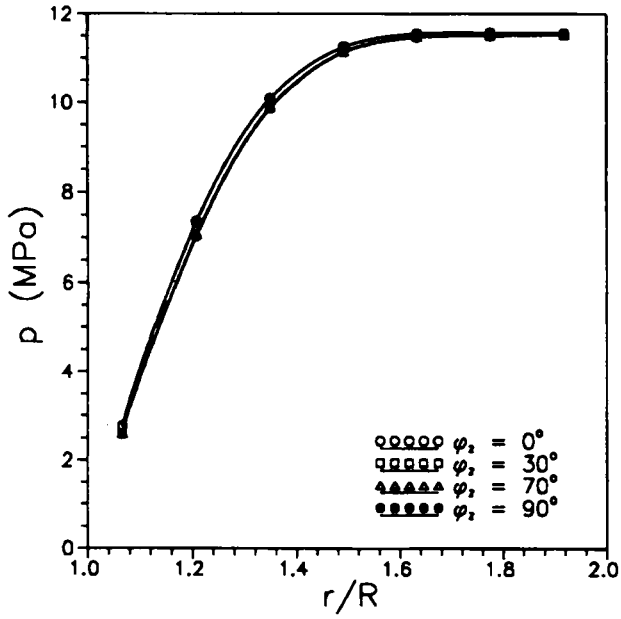

Figure 15. Effect of borehole inclination on pressure response, at $t = 5.28$ min, $\theta = 84.7°$, for anisotropic case

So far the total stresses were presented. For porous media, various physical phenomena are tied to the "effective stresses". It has been demonstrated in laboratory tests that the onset of material failure is associated with the Terzaghi's effective stress, rather than the Biot's effective stress. In Figure 8 and, the effective compressive radial stress $-\sigma_r'$, where $\sigma_r' = \sigma_r + p$, is plotted at $\theta = 6{\cdot}2°$. Note that the value above zero marks compression, while that below zero corresponds to tension. The result clearly shows a tensile region near the wellbore at small times. This type of pore pressure-induced effective tensile stress has been demonstrated in a plane strain vertical borehole solution.[6] and was reported to be the cuase of the 'outburst' events in coal.[33]

Next the anisotropic material case is investigated. The pore pressure profiles at the two azimuthal angles are exhibited as Figures 9 and 10. For easy comparison, the isotropic solution shown in Figures 5 and 6 are replotted here, yet with a different range, $1 \leqslant r/R \leqslant 2$, to enhance the near-field variation. Notice that the pore pressure is more affected by anisotropy in the 6·2° than in the 84·7° direction. Indeed, during the inclination, the permeability in the 90° direction remains unchanged and takes the horizontal permeability value, while in the 0° direction the permeability is a combination of the vertical and horizontal permeability which decreases with increasing inclination.

The effective radial stress at $\theta = 6{\cdot}2°$ is demonstrated in Figure 11. A comparison with the isotropic case shows that the material anisotropy enhances the effective tensile stress quite significantly. At $\theta = 84{\cdot}7°$, the difference of effective radial stress is relatively small between the isotropic and anisotropic cases. This result is hence not shown.

All the previous results are presented at a borehole inclination angle $\varphi_z = 70°$. To assess the effect of borehole inclination, in Figure 12, the pore pressure response at $t = 5{\cdot}28$ min, $\theta = 6{\cdot}2°$, and four different inclination angles, 0 (vertical), 30 and 70 and 90° (horizontal) were examined, for the isotropic material case. It is shown that the inclination increases the pore pressure magnitude. This is likely to be the consequence of the extra pore pressure generated by the

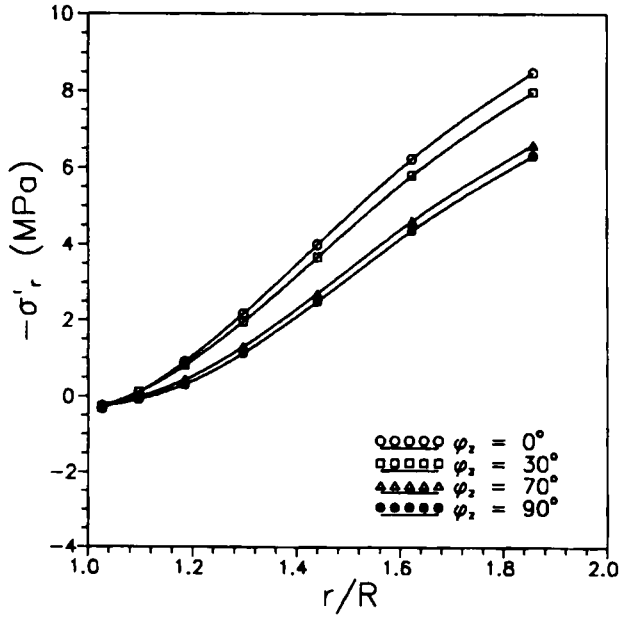

Figure 16. Effect of borehole inclination on effective compressive radial stress, at $t = 5.28$ min, $\theta = 6.2°$, for isotropic case

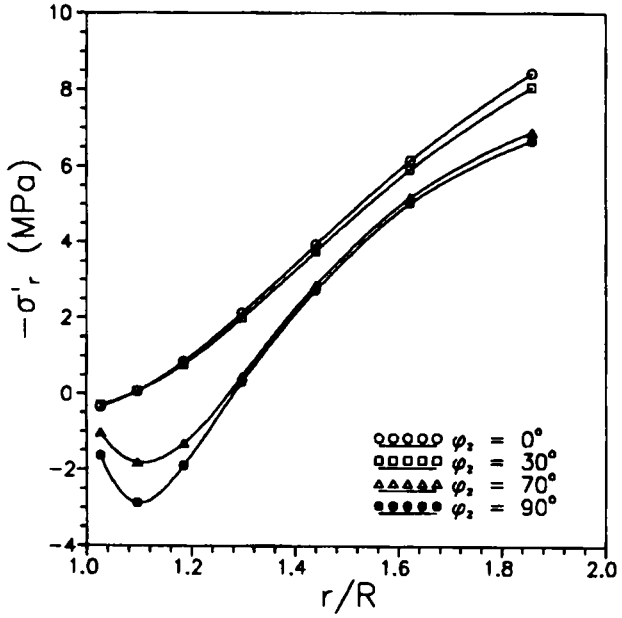

Figure 17. Effect of borehole inclination on effective compressive radial stress, at $t = 5.28$ min, $\theta = 6.2°$ for anisotropic case

Skempton's effect – at $\varphi_z = 0°$ the relevant far-field compressive stress at $\theta = 0°$ is $S'_y = 20$ MPa, which is changed to $S'_z = 25$ MPa at $\varphi_z = 90°$. Figure 13 shows the same pore pressure response, but at the azimuthal angle $\theta = 84{\cdot}7°$. In this case, the trend is reversed: pressure decreases with increasing inclination. While the relevant far-field compressive stress at $\theta = 90°$ reduces from $S'_x = 29$ MPa to $S'_z = 25$ MPa with a 90° inclination. The anisotropic cases at $\theta = 6{\cdot}2°$ and $84{\cdot}7°$ are, respectively, shown as Figures 14 and 15. The pressure magnitudes are apparently different from those of the isotropic cases. Figure 14 reveals a similar trend as Figure 12 in response to borehole inclination. However, due to the decreasing permeability in the x-direction as the borehole turns horizontal, the last two curves $\varphi_z = 70$ and 90° for the anisotropic case show higher pressure magnitude. In Figure 15, the trend of pore pressure reduction with increasing inclination appears to be offset by the more restricted pore pressure dissipation, due to the smaller permeability in the perpendicular direction. As a consequence, there is little change in the pressure magnitude.

For the effective stresses, the effective compressive radial stress $-\sigma'_r$ is explored. Figure 16 shows the influence of inclination for the isotropic case at $\theta = 6{\cdot}2°$ and $t = 5{\cdot}28$ min. The inclination causes a reduction in compressive stress. The tensile stress region (negative $-\sigma'_r$ values) is insignificant at this time. We however recall that the tensile region is more pronounced at smaller time (see Figure 8). Figure 17 demonstrates the same result except that the material is anisotropic. It is clearly observed that at larger inclination angles the anisotropy creates a significant effective tensile stress region.

SUMMARY AND CONCLUSION

In this paper a FEM formulation for the anisotropic, incrementally non-linear poroelastic medium is shown. The emphasis is on the presentation of material anisotropy. First, the

anisotropy in the generalized Biot's effective stress coefficient, α, is correctly modelled. Next, the continuum mechanics coefficients appearing in the generalized Hooke's law are firmly connected to the engineering constants for the two special material anisotropy cases: orthotropy and transverse isotropy. In view of the difficulty in the measurement of the α tensor, formulas for its evaluation based on the microisotropy assumption are provided. A three-dimensional FEM program is coded.

To validate the FEM code, an extended Mandel problem is solved. The recently derived result[25] provides the only anisotropic porelastic exact solution that the authors are aware of. The FEM solution compares very well with the exact solution.

Next, the inclined borehole problem, which is of great importance to the petroleum industry, is investigated. The solution also starts with a verification with the isotropic analytical solution. The FEM solution is again shown to be excellent. The influence of material anisotropy and the borehole inclination is examined in some detail. Various effects, such as the increase or decrease in pore pressure response in different regions and at different times, the enhancement of effective tensile stress region with the implication of 'outburst' failure, the time-dependent changes in compressive effective stress with the possibility of delayed failure, are revealed.

In the current analyses, material anisotropy is shown to exert significant impact on the effective stress magnitude and distribution, especially at large borehole inclination angles. This is contrary to the findings of elastic stress analysis[34] in which the anisotropy effect was found to be negligible if the degree of elastic anisotropy is not large, such as the case investigated here. For poroelasticity, it appears that the dominating factor is the permeability anisotropy which brings large pore pressure contrast, especially at large inclination angle. It is obvious that the effective stress will be significantly affected by the differences in pore pressure magnitude, even without the coupling effect. With the poroelastic coupling, a number of non-monotonic responses are further demonstrated.

In conclusion, a FEM code was built which is capable of solving quasi-static geomechanical problems in which the pore pressure effects are important. Although only material anisotropy is investigated in the examples in this paper, the program is fully capable of dealing with material incremental non-linearity. The original motivation for constructing such a program is for petroleum engineering applications, in particular, the stability of the drilling of inclined boreholes. The non-linearity and the stability issues of such problems are currently being investigated.

ACKNOLEDGEMENT

The work reported herein was supported in part by the Rock Mechanics Consortium and the Rock Mechanics Research Center at the University of Oklahoma.

REFERENCES

1. M. A. Biot, 'General theory of three dimensional consolidation,' *J. Appl. Phys.* **12**, 155–164 (1941).
2. J. Mandel, 'Consolidation des sols (étude mathématique),' *Géotechnique*, **3**, 287–299 (1953).
3. C. W. Cryer, 'A comparison of the three-dimensional consolidation theories of Biot and Terzaghi,' *Quart. J. Mech. Appl. Math.*, **16**, 401–412 (1963).
4. E. Detournay and A. H-D. Cheng, 'Pororelastic response of a borehole in a non-hydrostatic stress field,' *Int. J. Rock Mech. Min. Sci. Geomech. Abstr.*, **25**, 171–182 (1988).
5. E. Detournay, A. H-D. Cheng, J.-C. Roegiers and J. D. McLennan, 'Poroelasticity considerations in *in situ* stress determination by hydraulic fracturing,' *Int. J. Rock Mech. Mining Sci. Geomech. Abstr.*, **26**, 507–513 (1989).
6. A. H-D. Cheng, Y. Abousleiman and J.-C. Roegiers, 'Review of some poroelastic effects in rock mechanics,' *Int. J. Rock Meck. Min. Sci. Geomech. Abstr.*, **30**, 1119–1126 (1993).

7. E. Detournay and A. H-D. Cheng, 'Plane strain analysis of a stationary hydraulic fracture in a poroelastic medium,' *Int. J. Solids Struct.*, **37**, 1645–1662 (1991).
8. R. S. Sandhu and E. L. Wilson, 'Finite-element analysis of seepage in elastic Media,' *J. eng. mech. div. ASCE.*, **95**, 641–652 (1969).
9. J. Ghaboussi and E. L. Wilson, 'Flow of compressible fluid in porous elastic media', *Int. j. numer. methods eng.*, **5**, 419–442 (1973).
10. O. C. Zienkiewicz and T. Shiomi, 'Dynamic behaviour of saturated porous media: the generalized Biot formulation and its numerical solution,' *Int. j. numer. anal. methods geomech.*, **8**, 71–79 (1984).
11. R. W. Lewis and B. A. Schrefler, *The Finite Element Method in the Deformation and Consolidation of Porous Media*, Wiley, New York, 1987.
12. R. M. Sullivan and N. J. Salamon, 'A finite element method for the thermochemical decomposition of polymeric materials—I. Theory,' *Int. J. Eng. Sci.*, **30**, 431–441 (1992).
13. M. M. Carroll, 'An effective stress law for anisotropic elastic deformation,' *J. Geophys. Res.*, **84**, 7510–7512 (1979).
14. M. Thompson and J. R. Willis, 'A reformulation of the equations of anisotropic poroelasticity,' *J. appl. mech. ASME.*, **58**, 612–616 (1991).
15. S. P. Timoshenko and J. N. Goodier, *Theory of Elasticity*, *3rd edn.*, McGraw-Hill, New York, 1970.
16. L. Cui, Prorelasticity with application to rock mechanics, *Ph.D. Thesis*, University of Delaware, 1995.
17. O. C. Zienkiewicz and R. L. Taylor, *The Finite Element Method*, *4th edn*, McGraw-Hill, New York, 1989.
18. M. A. Biot, 'Theory of Elasticity and consolidation for a porous anisotropic solid,' *J. Appl. Phys.*, **26**, 182–185 (1955).
19. S. G. Lekhnitskii, *Theory of Elasticity of an Anisotropic Body* (transl. rev. 1977 Russian ed.) Mir, Moscow, 1981.
20. W.-F. Chen and A. F. Saleeb, *Constituttive Equations for Engineering Materials*, Vol. I, Wiley, New York, 1982.
21. M. A. Biot and D. G. Willis, 'The elastic coefficients of the theory of consolidation,' *J. Appl. Mech.*, **24**, 594–601 (1957).
22. E. Detournay and A. H.-D. Cheng, Fundamental of poroelasticity, in C. Fairhurst (ed.), *Comprehensive Rock Engineering: Principles, Practice and Projects*, Vol. II, *Analysis and Design Methods* Chap. 5, Pergamon Press, Oxford, 1993, pp. 113–171.
23. Y. Abousleiman, R. Chhajlani and J.-C. Roegiers, 'Effect of stress variation on Biot's parameter,' *Proc. 1st North American Rock Mech. Symp., Abstracts*, 1994, pp. 1–4.
24. A. H-D. Cheng and E. Detournay, 'A direct boundary element method for plane strain poroelasticity,' *Int. j. numer. analy. meth. geomech.*, **12**, 551–572 (1988).
25. Y. Abousleiman, A. H-D. Cheng, L. Cui, E. Detournay and J.-C. Roegiers, 'Mandel's problem revisted,' *Géotechnique*, in press.
26. B. S. Aadnoy and M. E. Chenevert, 'Stability of highly inclined boreholes,' *SPE Drill Eng.*, **2**, 364–374 (1987).
27. S. H. Ong and J.-C. Roegiers, 'Influence of anisotropies in borehole stability,' *Int. J. Rock Mech. Min. Sci. Geomech. Abstr.*, **30**, 1069–1075 (1993).
28. E. Fjær, R. M. Holt, P. Hosrud, A. M. Raaen and R. Risnes, *Petroleum Related Rock Mechanics*, Elsevier, Amsterdam, 1992.
29. T. Aoki, C. P. Tan and W. E. Bamford, 'Effects of elastic and strength anisotropy on borehole failures in saturated rocks,' *Int. J. Rock Mech. Min. Sci Geomech. Abstr.*, **30**, 1031–1034 (1993).
30. P. C. Shah, D. K. Gupta, S. Lehmar and B. G. Deruyck, 'A field application of the methodology for interpretation of horizontal well transient tests,' SPE 20611, *Ann. Tech. Conf. Exhib.*, 1990, pp. 865–876.
31. M. D. Zuber, J. C. Deters Jr. and W. J. Lee, 'A practical approach for analysis of a pressure transient test from a horizontal well in a gas storage reservoir,' SPE 22675, *Ann. Tech. Conf. Exhib.*, (1991, pp. 165–176.
32. L. Cui, A. H-D. Cheng and Y. Abousleiman, 'Poroelastic solution of an inclined borehole,' *J. appl. mech. ASME*, to appear.
33. L. Paterson, 'A model for outbursts in coal,' *Int. J. Rock. Mech. Min. Sci. Geomech. Abstr.*, **23**, 327–332 (1986).
34. B. S. Aadnoy, 'Modeling of the stability of highly inclined boreholes in anisotropic rock formations,' *SPE Drilling Eng.*, **3**, 259–268 (1988).